J Nanostruct 16(4): 5835-5849, Autumn 2026

RESEARCH PAPER

Design, Synthesis, and Mucus Penetrating Inhalable Lipid Polymer Hybrid Nanoparticles of Pyrroloquinazolinediamine DHFR Inhibitors for Targeted Treatment of Multidrug Resistant Pseudomonas aeruginosa Lung Infection

Hiba H. Rawdhan Al Badri [1]***, Ali S Abdalameer Allateef*** [2]***, Mohammed S Hashim Almatwari*** [3]***, Ali K Hoshi*** [3]***, Qutaiba A. Qasim*** [4]*

[1] *Department of Pharmaceutical Chemistry, College of Pharmacy, Al-Kunooze University, Basra, Iraq*

[2] *Department of Pharmaceutics, College of Pharmacy, Al-Kunooze University, Basra, Iraq*

[3] *Department of Pharmacology and Toxicology, College of Pharmacy, Al-Kunooze University, Basra, Iraq*

[4] *Department of Clinical Laboratory Sciences, College of Pharmacy, University of Basrah, Basrah, Iraq*

ARTICLE INFO

Article History:
Received 03 August 2026
Accepted 27 September 2026
Published 01 October 2026

Keywords:
Antimicrobial resistance
Inhalable formulation
Lipid–polymer hybrid nanoparticles
Mucus-penetrating particles
Pulmonary drug delivery

ABSTRACT

Biofilms formed by *Pseudomonas aeruginosa* promote the production of large amounts of dense, negatively charged airway mucus, which can impair the penetration and reduce the effective concentration of inhaled antimicrobials at the site of infection. This presents a particularly significant therapeutic challenge in chronic lung infections caused by multidrug-resistant (MDR) *P. aeruginosa*, a common pathogen associated with persistent and difficult-to-treat respiratory infections. Pyrroloquinazolinediamine (PQD)-based dihydrofolate reductase (DHFR) inhibitors represent a structurally distinct class of antifolates with potent activity against Gram-negative bacteria. However, their poor aqueous solubility and tendency to bind to mucus limit their suitability for inhaled drug delivery. In this study, we report the design, synthesis, and evaluation of lipid–polymer hybrid nanoparticles (LPHNPs) incorporating a lead PQD-based DHFR inhibitor, with the aim of overcoming these limitations by enhancing mucus penetration and enabling pulmonary administration via inhalation. The lead compound exhibited potent nanomolar inhibitory activity against bacterial DHFR while demonstrate high selectivity over human DHFR. Drug-loaded LPHNPs, consisting of a poly(lactic-co-glycolic acid) (PLGA) core, a phospholipid interfacial layer, and a dense corona of low-molecular-weight poly(ethylene glycol) (PEG), were developed using a Box–Behnken-optimized nanoprecipitation–self-assembly process. The optimized mucus-penetrating particles (MPPs) exhibited a mean diameter of 148.6 ± 4.2 nm, a near-neutral zeta potential of −7.8 mV, and an encapsulation efficiency of 82.4%. Drug release followed a biphasic profile governed by Fickian diffusion. Multiple-particle tracking studies demonstrated that the effective diffusion coefficient of the optimized MPPs was approximately 12-fold higher in a reconstituted cystic fibrosis mucus model compared with their non-PEGylated counterparts. Following nebulization, the MPPs exhibited a fine-particle fraction of 62.4% and a mass median aerodynamic diameter of 3.9 µm, indicating their suitability for pulmonary delivery. Notably, MPP formulation reduced the minimum inhibitory concentrations (MICs) and biofilm eradication concentrations (BECs) by up to eight-fold compared with the free drug against both reference strains and MDR clinical isolates. Furthermore, the formulation demonstrated no detectable cytotoxicity toward human airway epithelial cells. Collectively, these findings highlight mucus-penetrating LPHNPs as a promising strategy for the pulmonary delivery of PQD-based DHFR inhibitors against MDR P. aeruginosa infections.

How to cite this article
Al Badri H., Allateef A., Almatwari M., Hoshi A., Qasim Q. Design, Synthesis, and Mucus Penetrating Inhalable Lipid Polymer Hybrid Nanoparticles of Pyrroloquinazolinediamine DHFR Inhibitors for Targeted Treatment of Multidrug Resistant Pseudomonas aeruginosa Lung Infection. J Nanostruct, 2026; 16(4):5835-5849. DOI: 10.22052/JNS.2026.04.112

* *Corresponding Author Email: qutaiba.qasim@uobasrah.edu.iq*

This work is licensed under the Creative Commons Attribution 4.0 International License.
To view a copy of this license, visit http://creativecommons.org/licenses/by/4.0/.

INTRODUCTION

Gram-negative non-fermenting bacteria are at the forefront of the antimicrobial resistance crisis, representing one of the most pressing public health challenges of this decade. Carbapenem-resistant *Pseudomonas aeruginosa* (CRPA) was included in the World Health Organization's (WHO) 2024 Bacterial Priority Pathogens List, underscoring the urgent global need for effective therapeutic options capable of overcoming its extensive resistance mechanisms [1]. Resistance to multiple first-line antimicrobial classes is common among *P. aeruginosa* isolates, reflecting the remarkable capacity of this pathogen to acquire and regulate resistance determinants. This intrinsic and acquired resistance is further facilitated by the low permeability of its outer membrane, together with constitutively expressed and inducible efflux mechanisms [2, 3]. Moreover, its metabolic and regulatory flexibility enables *P. aeruginosa* to survive under adverse environmental conditions and transition between acute and chronic infection states in response to antimicrobial treatment and changes in the host environment [4]. This persistence is particularly pronounced in the respiratory tract, where *P. aeruginosa* can colonize the airways, establish long-term pulmonary infections, and progressively develop antibiotic tolerance. In individuals with cystic fibrosis (CF) and other suppurative lung diseases, the pathogen can adopt a mucoid phenotype and form biofilms, adaptations that are particularly suited to the airway environment [5]. Within these biofilms, the extracellular polymeric matrix and the altered microenvironment impair antimicrobial penetration, reduce bacterial metabolic activity, and protect persister cells. Consequently, antimicrobial concentrations that are lethal to planktonic bacteria may have limited efficacy against bacteria residing within the sessile biofilm community. As a result, complete eradication of *P. aeruginosa* from the respiratory tract is rarely achieved, and chronic infections often require repeated courses of high-dose antimicrobial therapy, further promoting the selection and emergence of resistant bacterial populations [6, 7]. A second, less widely recognized barrier to effective antimicrobial delivery against biofilms is the airway mucus layer itself. The high viscoelasticity, dehydration, and dense network of cross-linked mucins, extracellular DNA, and other polyanionic components in CF sputum, combined with its ability to efficiently trap foreign particles through steric obstruction and adhesive interactions, account for its strong particle-trapping properties [8]. Consequently, most inhaled antibiotics and conventional nanoparticles become entrapped within the outer mucus layer and are cleared before reaching the airway epithelium and underlying biofilm, thereby limiting local drug availability following pulmonary administration [8, 9]. It has become increasingly evident that particle surface chemistry plays a critical role in determining transport through mucus. Accordingly, coating particle surfaces with a dense corona of low-molecular-weight poly(ethylene glycol) (PEG) can minimize adhesive interactions with mucus components and facilitate particle diffusion at rates approaching those observed in water. This principle underlies the development of mucus-penetrating particles (MPPs) [9, 10]. Importantly, PEG chain length and surface grafting density are critical determinants of mucus transport, and their optimization requires a careful balance between minimizing mucoadhesive interactions and maintaining effective mucus penetration rather than assuming that PEGylation alone is sufficient [10-13].

Meanwhile, the stagnation of the antibacterial drug development pipeline has renewed interest in previously validated but underexploited therapeutic targets. One such target is dihydrofolate reductase (DHFR), an enzyme that catalyses the NADPH-dependent reduction of dihydrofolate to tetrahydrofolate, an essential cofactor for the de novo synthesis of thymidylate, purines, and several amino acids. Inhibition of DHFR disrupts these essential biosynthetic pathways, thereby impairing DNA replication and ultimately exerting bactericidal activity [14]. Trimethoprim is the prototypical antibacterial DHFR inhibitor; however, its clinical effectiveness has been compromised by the widespread emergence of resistance, primarily through mutations in the target enzyme and the acquisition of mobile *dfr* genes, both of which reduce or prevent effective drug binding [14, 15]. These limitations have prompted the search for alternative chemical scaffolds capable of inhibiting resistant DHFR variants. Among the emerging candidates, pyrroloquinazolinediamine (PQD) represents a particularly promising antifolate scaffold. PQD derivatives exhibit nanomolar inhibitory activity against bacterial DHFR and retain activity against Gram-negative

CC BY

bacteria resistant to trimethoprim. Unlike classical diaminopyrimidines, these compounds interact with the target enzyme through a distinct binding mode. Furthermore, their additional effects on bacterial membrane integrity and biofilm formation suggest a potentially advantageous multi-mechanistic antibacterial profile, which may reduce the likelihood of resistance development [16]. The related PQD has also been investigated for its potential as an antimalarial antifolate [17]. The ability of PQD-based inhibitors to retain activity against multidrug-resistant (MDR) *P. aeruginosa* makes them promising candidates for the treatment of difficult-to-treat respiratory infections. However, like many promising antifolate lead compounds, they suffer from poor aqueous solubility. Moreover, their small-molecule nature provides no inherent mechanism for prolonged retention at the airway surface or protection against sequestration by the mucus barrier. Consequently, despite their promising antibacterial properties, effective pulmonary delivery of these compounds remains a significant formulation challenge. Lipid–polymer hybrid nanoparticles (LPHNPs) represent a promising drug delivery platform that can address many of the limitations associated with conventional delivery systems. These nanoparticles consist of a biodegradable polymeric core, typically composed of poly(lactic-co-glycolic acid) (PLGA), surrounded by a phospholipid shell. This hybrid structure combines the high drug-loading capacity and sustained-release properties of polymeric nanoparticles with the biocompatibility and tunable surface characteristics of liposomes, while minimizing aggregation and burst drug release, which are common challenges associated with single-component systems [18, 19]. The PLGA core provides a well-established matrix for controlled and sustained drug release [20], whereas the lipid interface offers anchoring sites for PEGylated phospholipids, such as DSPE-PEG. This enables the formation of a PEG-based surface corona through a single self-assembly step, potentially enhancing nanoparticle penetration through mucus barriers. Furthermore, pulmonary drug delivery represents a particularly attractive route for these nanocarriers, as it enables direct drug delivery to the site of infection, achieves high local drug concentrations, while minimizing systemic exposure, and bypasses first-pass metabolism [21, 22]. Nevertheless, despite the promising potential of pulmonary nanomedicine, successful pulmonary delivery requires nanoparticles to meet several critical criteria. These include an appropriate aerodynamic particle size (typically 1–5 µm), sufficient stability during aerosolization, and the ability to penetrate mucus and biofilm barriers before releasing their therapeutic cargo [23-25].

Although considerable research has been conducted on inhalable antibiotic nanocarriers and mucus-penetrating nanoparticles, the integration of these two approaches for the pulmonary delivery of a novel chemotype of dihydrofolate reductase (DHFR) inhibitor targeting *Pseudomonas aeruginosa* remains unexplored. Accordingly, we hypothesized that incorporating a lead PQD-based DHFR inhibitor into PEGylated LPHNPs would (i) protect the inhibitor and improve its solubility, (ii) enhance its transport across CF-like mucus, (iii) facilitate the generation of a respirable aerosol, and (iv) improve its antibacterial and antibiofilm efficacy against multidrug-resistant (MDR) clinical isolates while maintaining cytocompatibility with airway epithelial cells.

In the present study, we describe the design and synthesis of the lead compound, followed by the Box–Behnken experimental design for formulation optimization and the physicochemical characterization of drug-loaded, mucus-penetrating LPHNPs. Furthermore, we investigate their in vitro drug-release profiles, mucus-penetration capacity, and aerodynamic performance, as well as their antibacterial and antibiofilm activities and cytocompatibility. These properties are evaluated in comparison with those of the free drug and non-PEGylated hybrid nanoparticles.

MATERIALS AND METHODS

Materials

Poly(D,L-lactide-co-glycolide) (PLGA 50:50, ester-terminated, inherent viscosity of 0.17–0.24 dL g^{-1}), soybean L-α-phosphatidylcholine (lecithin), and 1,2-distearoyl-sn-glycero-3-phosphoethanolamine-N-[methoxy(polyethylene glycol)-2000] (DSPE-PEG2000) were used as the polymeric core, interfacial lipid, and PEGylated lipid components, respectively. The lead pyrroloquinazolinediamine compound, type II mucin (porcine gastric mucin), components of the reconstituted CF-like mucus model, bacteriological culture media, resazurin, crystal violet, and the

CC BY

tetrazolium-based cell viability reagent were of analytical grade. Ultrapure water with a resistivity of 18.2 MΩ·cm was used throughout all experimental procedures. Detailed information regarding reagent identities, grades, and instrument settings is provided in the Appendix.

Design and synthesis of the lead PQD DHFR inhibitor

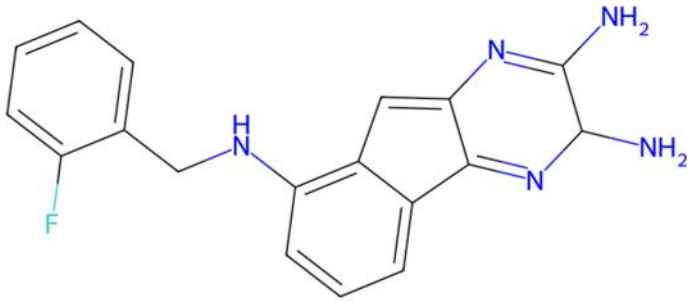
The lead inhibitor (PQD-L, Fig. 1), a 1,3-diamino-7H-pyrrolo[3,2-f]quinazoline derivative bearing a 2-fluorobenzyl substituent at the pyrrole nitrogen, was selected to achieve favorable DHFR binding, while retaining the membrane-perturbing properties reported for this class of compounds [26]. The pyrrolo[3,2-f]quinazoline-1,3-diamine core of PQD-L was synthesized using a convergent synthetic strategy, starting from a functionalized anthranilonitrile. The 1,3-diamino functionality was subsequently introduced through guanylation and cyclization reactions, followed by a final deprotection step. The crude product was purified by flash chromatography and recrystallization. Its identity and purity were confirmed by $^{1}H/^{13}C$ NMR spectroscopy and high-resolution mass spectrometry (HRMS), with the purity exceeding 98% as determined by HPLC. A concise overview of the synthetic procedures, key intermediates, and characterization criteria is provided in the Appendix.

DHFR inhibition and selectivity

Recombinant *Pseudomonas aeruginosa* DHFR activity was evaluated using a spectrophotometric assay at 25 °C, monitoring NADPH oxidation at 340 nm in the presence of dihydrofolate and NADPH at fixed concentrations near their respective K_m values. Initial reaction velocities were determined across a range of inhibitor concentrations, and the corresponding half-maximal inhibitory concentrations (IC_{50}) were calculated by nonlinear regression analysis. The inhibitory activity against recombinant human DHFR was assessed using the same experimental procedure. Enzyme selectivity was expressed as the selectivity index (SI), calculated as the ratio of the IC_{50} value for human DHFR to that for bacterial DHFR. Trimethoprim was included as a reference inhibitor and internal assay control.

Preparation of lipid–polymer hybrid nanoparticles

A modified single-step nanoprecipitation and self-assembly technique was employed to prepare drug-loaded lipid–polymer hybrid nanoparticles (LPHNPs). Briefly, PLGA and PQD-L were dissolved in acetonitrile to form the organic phase. The aqueous phase consisted of a 4% (v/v) aqueous ethanol solution containing lecithin and DSPE-PEG2000, which was preheated to 65 °C. Under continuous magnetic stirring, the organic phase containing PLGA and the drug was added dropwise to the preheated lipid dispersion. This process induced nanoprecipitation of the polymeric core, followed by the self-assembly of lecithin and PEGylated lipid molecules around the core, resulting in the formation of LPHNPs with a lipid/PEG-lipid shell. The resulting suspension was continuously stirred for 3 h to facilitate the removal of the organic solvent. Subsequently, the nanoparticles were purified by three successive



PQD-L

1,3-diamino-7-(2-fluorobenzyl)-7H-pyrrolo[3,2-f]quinazoline

Fig. 1. Chemical structure of the lead pyrroloquinazolinediamine DHFR inhibitor (PQD-L) used in this study.

CC BY

ultrafiltration cycles using a membrane with a molecular weight cut-off (MWCO) of 100 kDa and finally resuspended in the desired medium. Non-PEGylated conventional particles (CPP-PQD) were prepared using the same procedure, except that DSPE-PEG2000 was omitted. Blank nanoparticles (blank MPP) were prepared following the same protocol without incorporating the drug. Throughout this study, the nanoparticles are referred to as follows: MPP-PQD (PEGylated, mucus-penetrating nanoparticles), CPP-PQD (non-PEGylated conventional nanoparticles), and blank MPP (drug-free PEGylated nanoparticles).

Box–Behnken optimization

Formulation optimization and modelling of the effects of formulation variables on critical quality attributes (CQAs) were performed using a three-factor, three-level Box–Behnken design (BBD), consisting of 15 experimental runs, including three replicated centre points [27, 28]. The independent variables were the amount of PLGA (X_1, 10–30 mg), the lipid-to-polymer mass ratio (X_2, 0.10–0.20), and the proportion of DSPE-PEG2000 in the total lipid content (X_3, 10–30%). The selected responses were particle size (Y_1), polydispersity index (PDI; Y_2), and encapsulation efficiency (EE; Y_3). A second-order polynomial model was fitted to each response to evaluate the effects of the formulation variables and their interactions. The optimal formulation composition was determined using numerical desirability optimization, with the objectives of minimizing particle size and PDI while maximizing encapsulation efficiency.

Physicochemical Characterization

Particle size distribution was measured using dynamic light scattering (DLS), while the polydispersity index (PDI) was determined by electrophoretic light scattering (ELS) in 10 mM NaCl at 25 °C. The morphological characteristics of the nanoparticles were examined by transmission electron microscopy (TEM) following negative staining. The formation of a core–shell structure was inferred from the enhancement in particle size following lipid coating and the changes in zeta potential (ζ-potential) after PEGylation. Following ultrafiltration, encapsulation efficiency (EE) and drug loading (DL) were determined by quantifying the free and total drug content using a validated reversed-phase high-performance liquid chromatography (RP-HPLC) method. EE and DL were calculated according to the equations provided in the Appendix.

In-vitro drug release and kinetics

In vitro drug release was evaluated using the dialysis bag method with a molecular weight cut-off (MWCO) of 12–14 kDa. The release study was conducted in phosphate-buffered saline (PBS; pH 7.4) containing 0.5% (w/v) polysorbate 80 to maintain sink conditions. The experiment was performed at 37 °C under orbital agitation. At predetermined time intervals, aliquots of the release medium were withdrawn and replaced with equal volumes of fresh, pre-warmed medium to maintain constant release conditions. The amount of released drug was quantified using high-performance liquid chromatography (HPLC). Solubilized free PQD-L was used as a control.

The cumulative drug release profiles were fitted to zero-order, first-order, Higuchi, and Korsmeyer–Peppas kinetic models. The best-fitting model was identified based on the coefficient of determination (R^2), while the drug release mechanism was assessed using the release exponent (n) obtained from the Korsmeyer–Peppas model [29].

Mucus-penetration study

The transport of nanoparticles through a reconstituted CF mucus model and porous mucin gels was investigated. Fluorescently labelled MPP-PQD and CPP-PQD nanoparticles were incorporated into the gel matrices, and the Brownian motion trajectories of individual particles were recorded using video microscopy at a frame rate of 30 frames per second. Time-averaged mean-squared displacement (MSD) values were calculated as a function of lag time, and ensemble-averaged effective diffusion coefficients (D_eff) were determined at a lag time of 1 s. These values were then compared with the theoretical diffusion coefficient in water (D_w) for particles of equivalent size. In addition, the fractions of mobile particles and particles capable of penetrating beyond a depth of 10 μm were quantified [30].

Aerodynamic performance

The aerosolization performance of the nebulized suspensions was evaluated using a vibrating-mesh nebulizer coupled to a Next Generation Impactor (NGI) operated at a flow rate of 15 L/min [31]. The drug deposited in the induction port and on each

(cc) BY

impactor stage was recovered and quantified using HPLC. The mass median aerodynamic diameter (MMAD) and geometric standard deviation (GSD) were determined from the cumulative drug deposition as a function of the effective cut-off diameter. The fine-particle fraction (FPF), defined as the fraction of the emitted dose with an aerodynamic diameter of less than 5 µm, and the emitted dose (ED) were calculated according to the equations provided in the Appendix.

Antibacterial and antibiofilm activity

The minimum inhibitory concentrations (MICs) and minimum bactericidal concentrations (MBCs) were determined using standard reference methods against *P. aeruginosa* strains PA14 and PAO1, as well as three multidrug-resistant (MDR) clinical isolates (PA-MDR-01, PA-MDR-02, and PA-MDR-03). Trimethoprim was included as a comparator [32]. All concentrations were expressed as PQD-equivalent concentrations. The antibiofilm activity of the formulations was evaluated against 24-h-old biofilms using the peg-lid biofilm model. The minimum biofilm inhibitory concentration (MBIC) and minimum biofilm eradication concentration (MBEC) were determined by following treatment at concentrations equivalent to four times the planktonic MIC. Biofilm biomass was quantified by crystal violet staining, while bacterial viability was assessed by determining viable colony counts [33, 34]. Free PQD-L, CPP-PQD, and blank MPP were included in the experiments.

Cytocompatibility

Cytotoxicity was evaluated following 24 h of exposure of human lung epithelial cell lines (Calu-3 and A549) to MPP-PQD, free PQD-L, and blank MPP at concentrations ranging from 5 to 100 µg/mL (expressed as PQD-equivalent concentrations). Cell viability was assessed using a tetrazolium-based reduction assay. The results were expressed as percentages of the viability of untreated control cells, and the half-maximal cytotoxic concentration (CC_{50}) values were determined by interpolation. Haemocompatibility was assessed by measuring haemoglobin release from human erythrocytes as an indicator of haemolysis.

RESULTS AND DISCUSSION

Synthesis and target engagement

The overall yield of the synthetic sequence was 22%. The lead pyrroloquinazolinediamine compound, PQD-L, exhibited a chromatographic purity of greater than 98%, and its spectroscopic characteristics were consistent with the structure of 1,3-diamino-7H-pyrrolo[3,2-f]quinazoline. PQD-L demonstrated potent inhibitory activity against recombinant *Pseudomonas aeruginosa* dihydrofolate reductase (DHFR), with an IC_{50} value of 9.2 ± 1.1 nM, compared with 4.6 ± 0.5 µM for trimethoprim. In contrast, its inhibitory activity against human DHFR was considerably lower, with an IC_{50} value of 3.4 ± 0.4 µM, corresponding to a selectivity index of approximately 370 in favour of the bacterial enzyme. These findings demonstrate the potent nanomolar inhibition of bacterial DHFR

Table 1. Box–Behnken design matrix and observed responses.

Run	X_1 PLGA (mg)	X_2 Lipid:Polymer	X_3 DSPE-PEG (%)	Y_1 Size (nm)	Y_2 PDI	Y_3 EE (%)
1	10	0.10	20	132.4	0.171	71.8
2	30	0.10	20	171.9	0.198	84.6
3	10	0.20	20	149.7	0.205	74.9
4	30	0.20	20	188.3	0.224	86.1
5	10	0.15	10	151.2	0.212	72.4
6	30	0.15	10	190.6	0.229	85.9
7	10	0.15	30	128.7	0.152	70.6
8	30	0.15	30	166.5	0.170	82.7
9	20	0.10	10	158.9	0.201	79.2
10	20	0.20	10	176.4	0.222	80.8
11	20	0.10	30	139.1	0.149	78.1
12	20	0.20	30	152.8	0.166	79.7
13	20	0.15	20	148.9	0.163	82.3
14	20	0.15	20	147.6	0.159	82.6
15	20	0.15	20	149.4	0.165	81.9

Runs 13–15 are centre points. Values are single determinations per design run; the confirmatory optimum was measured in triplicate.

CC BY

by PQD-L, together with substantially reduced activity against the human enzyme, consistent with the previously reported antibacterial DHFR-targeting profile of the PQD compound class [16].

Formulation optimization

The effects of formulation composition on the critical quality attributes (CQAs) were evaluated using a Box–Behnken experimental design (Table 1). PLGA content and the lipid-to-polymer ratio exhibited positive effects on particle size, whereas increasing the DSPE-PEG2000 content resulted in reductions in both particle size and polydispersity index (PDI), which were attributed to improved interfacial stabilization. Increasing the PLGA content also enhanced encapsulation efficiency, presumably by providing a larger hydrophobic core for the incorporation of the lipophilic drug. However, encapsulation efficiency showed a slight decrease at the highest DSPE-PEG2000 concentrations. Numerical optimization identified the optimal formulation composition as 20 mg PLGA, a lipid-to-polymer ratio of 0.15, and 20% DSPE-PEG2000. A confirmatory batch was subsequently prepared using these optimized conditions. The experimentally observed responses were in close agreement with the model-predicted values, within the experimental error, thereby confirming the predictive reliability of the developed model.

Physicochemical properties

The optimized MPP-PQD formulation exhibited a monodisperse particle size distribution and a nearly spherical core–shell morphology (Fig. 2), with a low polydispersity index of 0.162 and a high encapsulation efficiency of 82.4% (Table 2). The primary difference between the mucus-penetrating and conventional formulations was their surface charge. PEGylation resulted in a near-neutral zeta potential of −7.8 mV for MPP-PQD, compared with −28.4 mV for CPP-PQD. This shift

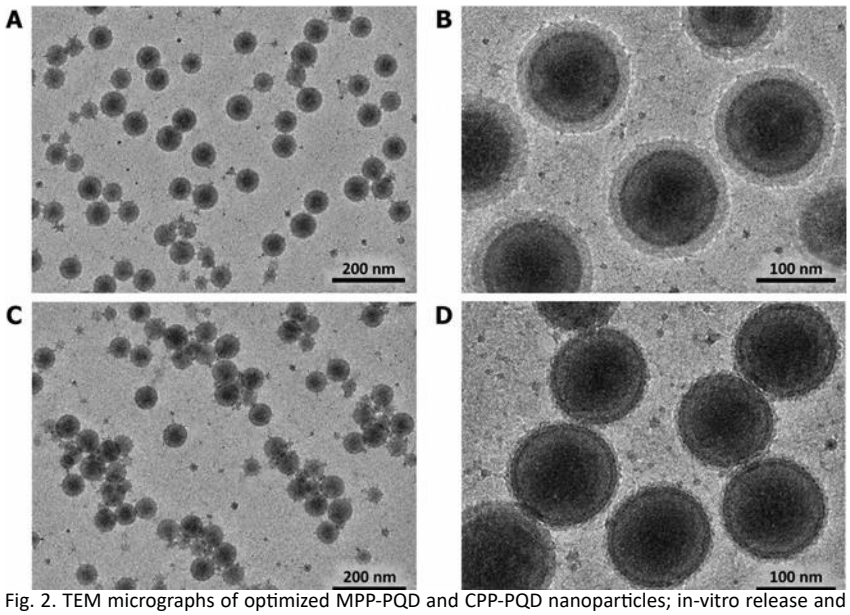


Fig. 2. TEM micrographs of optimized MPP-PQD and CPP-PQD nanoparticles; in-vitro release and kinetics.

Table 2. Physicochemical properties of optimized formulations (Mean ± SD, N = 3).

Formulation	Size (nm)	PDI	Zeta (mV)	EE (%)	DL (%)
MPP-PQD	148.6 ± 4.2	0.162 ± 0.018	−7.8 ± 1.1	82.4 ± 2.6	6.7 ± 0.4
CPP-PQD	155.3 ± 5.1	0.191 ± 0.021	−28.4 ± 2.3	79.1 ± 3.0	6.2 ± 0.5
Blank MPP	139.2 ± 3.8	0.148 ± 0.015	−6.9 ± 0.9		

CC BY

towards a less negative surface charge is indicative of effective PEG corona formation, which shields the negatively charged PLGA surface [11, 12]. Drug loading was comparable across all formulations, ranging from 6.2% to 6.7%. In addition, blank nanoparticles exhibited a slightly smaller particle size than their drug-loaded counterparts, which may be attributed to the additional volume occupied by the encapsulated drug within the nanoparticle core.

Both nanoparticle formulations exhibited biphasic drug release profiles, characterized by an initial burst release of surface-associated drug, followed by a sustained release phase. During the first 6 h, approximately 36% and 38% of the encapsulated drug was released from MPP-PQD and CPP-PQD, respectively. This initial phase was followed by a prolonged release phase, presumably governed by drug diffusion and polymer matrix erosion, with cumulative drug release reaching approximately 88% and 84% after 72 h for MPP-PQD and CPP-PQD, respectively. In contrast, free PQD-L was almost completely released within 8 h (Fig. 3). These findings indicate that nanoparticle encapsulation transformed PQD-L, a readily available small-molecule drug, into a sustained-release depot capable of maintaining drug release over a period of three days. Among the kinetic models evaluated, the Korsmeyer–Peppas model provided the best fit for both nanoparticle formulations, yielding the highest coefficients of determination (R^2 = 0.994 for both MPP-PQD and CPP-PQD). The corresponding release exponent (n) was approximately 0.43, indicating Fickian diffusion as the predominant drug release mechanism from the PLGA core (Table 3) [20, 29].

Mucus penetration

Multiple-particle tracking (MPT) revealed a pronounced influence of the PEG corona on nanoparticle transport through the reconstituted CF mucus model (Fig. 4 and Fig. 5, Table 4). MPP-PQD exhibited near-Brownian motion, with an ensemble-averaged effective diffusion coefficient (D_eff) of 4.6×10^{-2} μm²/s and a D_eff/D_w ratio of 0.021. In contrast, the non-PEGylated CPP-PQD particles displayed substantially restricted mobility, with a D_eff/D_w ratio of 0.0018, representing an approximately 12-fold difference in diffusivity in favour of the mucus-penetrating formulation.

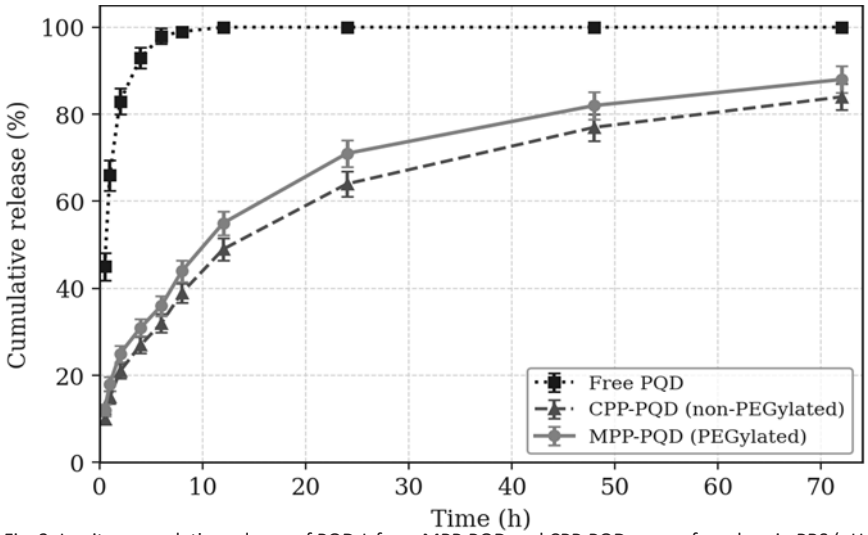


Fig. 3. In-vitro cumulative release of PQD-L from MPP-PQD and CPP-PQD versus free drug in PBS (pH 7.4, 37 °C). Data are mean ± SD (n = 3).

Table 3. Release-kinetic model fitting (coefficient of determination, R^2).

Formulation	Zero-order	First-order	Higuchi	Korsmeyer–Peppas	n
MPP-PQD	0.902	0.972	0.981	0.994	0.43
CPP-PQD	0.915	0.968	0.985	0.991	0.41

CC BY

Consistent with these findings, 68% of MPP-PQD particles penetrated beyond a mucus depth of 10 µm, compared with only 9% of CPP-PQD particles. Collectively, these results demonstrate that the near-neutral surface charge and dense PEG corona of MPP-PQD facilitate mucus penetration by reducing adhesive interactions with the mucus network and preventing the particle entrapment

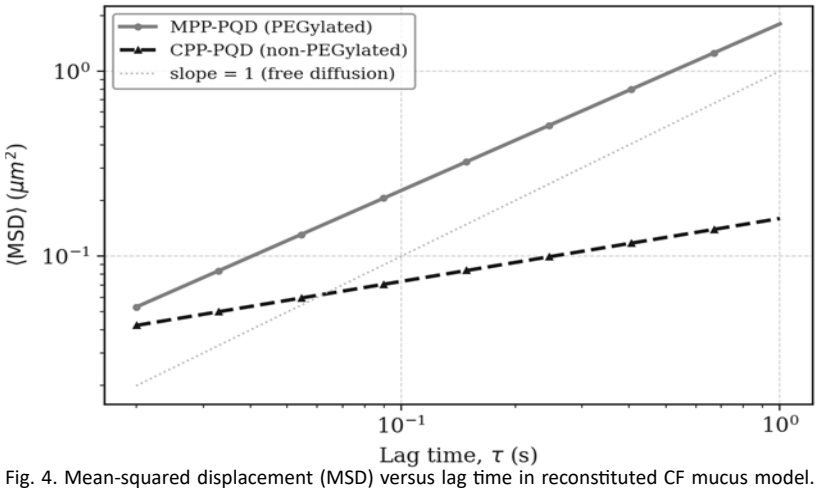


Fig. 4. Mean-squared displacement (MSD) versus lag time in reconstituted CF mucus model. The dotted line (slope = 1) denotes unobstructed diffusion.

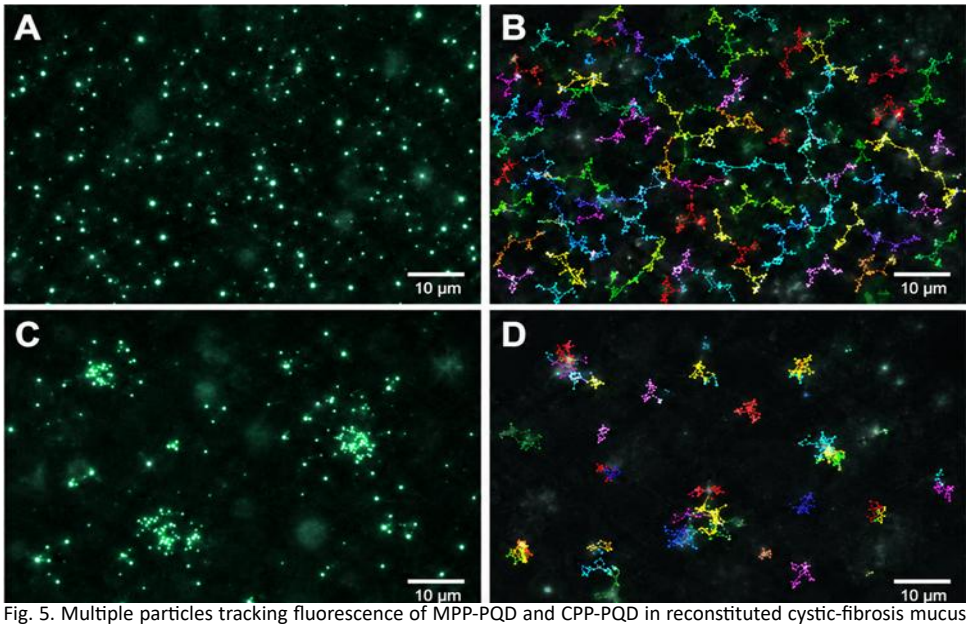


Fig. 5. Multiple particles tracking fluorescence of MPP-PQD and CPP-PQD in reconstituted cystic-fibrosis mucus model.

Table 4. Transport parameters in reconstituted cystic-fibrosis mucus model (Mean± SD, N = 3).

Formulation	$\langle MSD \rangle_{1s}$ (µm²)	D_eff (µm² s^{-1})	D_eff/D_w	Penetrating >10 µm (%)
MPP-PQD	1.82 ± 0.21	4.6×10^{-2}	0.021 ± 0.004	68 ± 6
CPP-PQD	0.15 ± 0.03	3.9×10^{-3}	0.0018 ± 0.0005	9 ± 3

CC BY

observed with conventional non-PEGylated nanoparticles [8-10].

Aerodynamic performance

The aerosol generated from nebulized MPP-PQD exhibited suitable aerodynamic characteristics for deep-lung deposition (Table 5). The mass median aerodynamic diameter was 3.9 µm, with a geometric standard deviation of 1.9, indicating that the majority of the emitted dose was within the 1–5 µm aerodynamic diameter range, which is considered suitable for deposition in the bronchiolar and alveolar regions [23, 24]. Furthermore, MPP-PQD demonstrated a fine-particle fraction (FPF) of 62.4% and an emitted dose (ED) of 88.7%. These values were higher than those obtained for CPP-PQD, which exhibited an FPF of 55.1% and an MMAD of 4.2 µm. Collectively, these findings indicate that PEGylation did not compromise nanoparticle stability during nebulization or adversely affect aerosol performance.

Antibacterial and antibiofilm activity

Regarding planktonic antibacterial activity, the potency of PQD-L was generally maintained following encapsulation, with MPP-PQD demonstrating improved activity against certain reference and multidrug-resistant (MDR) isolates (Table 6, Fig. 6). Specifically, MPP-PQD reduced the MIC by two-fold compared with the free drug for the MDR isolates, as exemplified by PA-MDR-03,

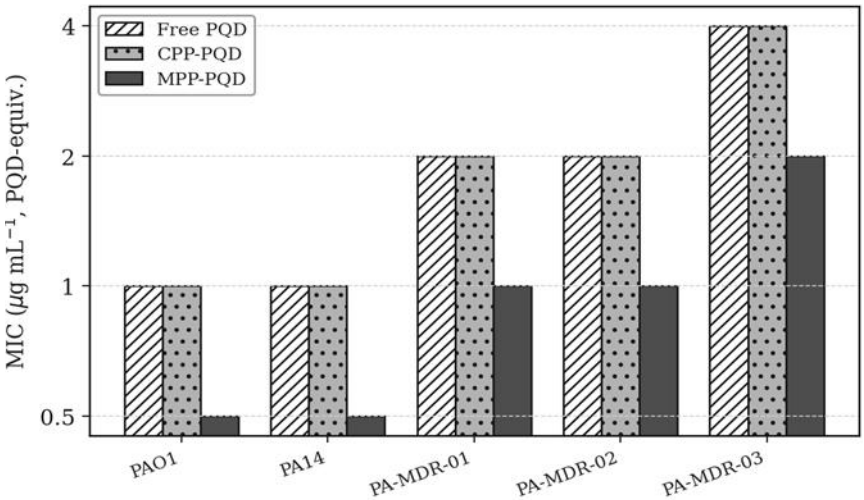


Fig. 6. MIC (PQD-equivalent) of free drug, CPP-PQD, and MPP-PQD against reference and MDR clinical isolates.

Table 5. Aerodynamic performance of nebulized formulations (Mean ± SD, N = 3).

Formulation	MMAD (µm)	GSD	FPF (<5 µm, %)	Emitted dose (%)
MPP-PQD	3.9 ± 0.3	1.9 ± 0.1	62.4 ± 3.1	88.7 ± 2.4
CPP-PQD	4.2 ± 0.4	2.0 ± 0.2	55.1 ± 3.6	85.3 ± 2.9

Table 6. MIC and MBC against *P. aeruginosa* strains (µg/mL, PQD-equivalent).

Strain	Free MIC	CPP MIC	MPP MIC	MPP MBC	TMP MIC	Phenotype
PAO1	1	1	0.5	1	16	Reference
PA14	1	1	0.5	2	32	Reference
PA-MDR-01	2	2	1	2	>128	MDR
PA-MDR-02	2	2	1	4	>128	MDR
PA-MDR-03	4	4	2	4	>128	XDR

CC BY

for which the MIC decreased from 4 to 2 µg/mL. However, the MIC against the reference isolates remained comparable to that of the free drug. Notably, all MDR isolates exhibited resistance to trimethoprim, with MIC values exceeding 128 µg/mL, highlighting the potential value of PQD-L as an alternative antibacterial chemotype. Bactericidal activity was observed at concentrations approximately 100–400 times higher than the MIC, with MBC values generally following the same trend as the corresponding MIC values.

The benefits of the mucus-penetrating

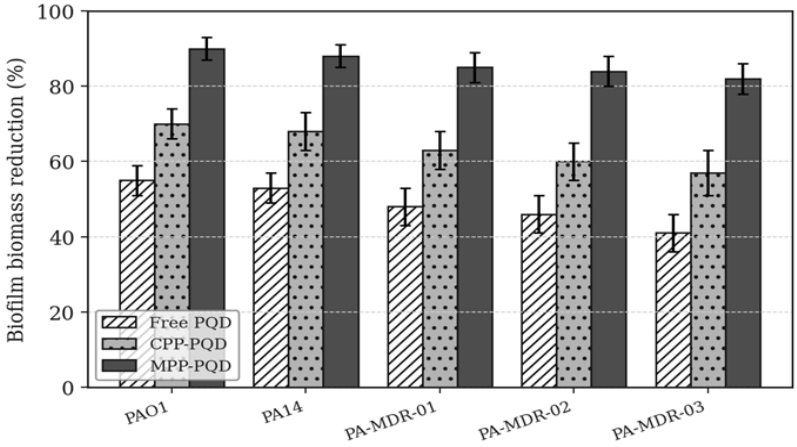


Fig. 7. Biofilm biomass reduction at 4× MIC (crystal-violet assay). Data are mean ± SD (n = 3).

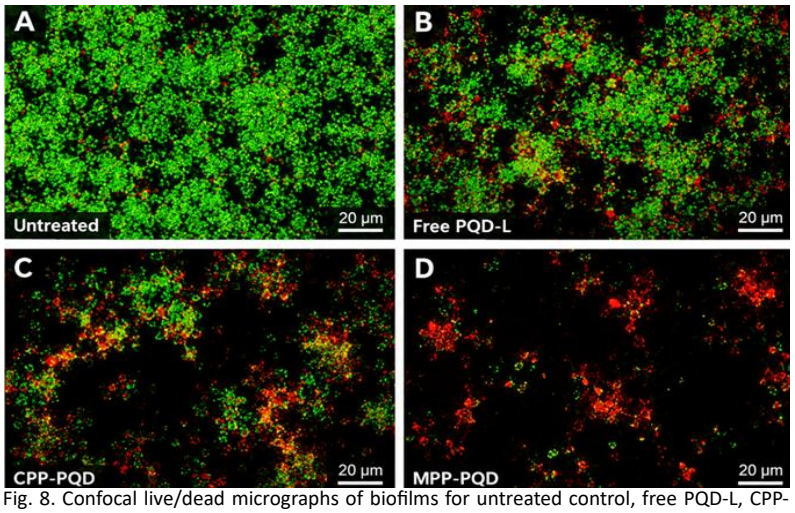


Fig. 8. Confocal live/dead micrographs of biofilms for untreated control, free PQD-L, CPP-PQD, and MPP-PQD.

Table 7. Antibiofilm activity (Mean ± SD, N = 3).

Strain	MBEC Free	MBEC MPP	Biomass ↓ MPP (%)	Log_{10} CFU ↓ MPP
PAO1	32	8	90 ± 3	3.8 ± 0.3
PA14	32	8	88 ± 3	3.6 ± 0.3
PA-MDR-01	64	16	85 ± 4	3.3 ± 0.4
PA-MDR-02	64	16	84 ± 4	3.1 ± 0.4
PA-MDR-03	>128	32	82 ± 4	2.9 ± 0.4

MBEC in µg/mL (PQD-equivalent). Biomass reduction and log-kill measured at 4× planktonic MIC after 24 h exposure.

CC BY

nanoparticle design were particularly pronounced in the treatment of bacterial biofilms (Table 7, Fig. 7, Fig. 8). Compared with the free drug, MPP-PQD reduced the minimum biofilm eradication concentration by 4–8-fold against *P. aeruginosa* PAO1. Furthermore, at a concentration equivalent to four times the planktonic MIC, MPP-PQD reduced viable bacterial counts by up to 3.8 log_{10} and decreased biofilm biomass by 82–90%. In contrast, free PQD-L achieved only a 1.9-log_{10} reduction in viable counts and a 41–55% reduction in biofilm biomass under the same treatment conditions. CPP-PQD exhibited intermediate antibiofilm activity, potentially reflecting its limited penetration into the biofilm matrix. Collectively, these findings suggest that the combination of sustained drug release, enhanced penetration through the mucus and biofilm matrices, and the intrinsic antibiofilm activity of the PQD scaffold contribute to the more effective elimination of biofilm-associated bacterial populations by MPP-PQD.

Cytocompatibility and enzyme selectivity

MPP-PQD exhibited a favourable cytocompatibility profile in human airway epithelial cells, with cell viability remaining above 85% across the tested conditions (Table 8, Fig. 9). The interpolated half-maximal cytotoxic concentration (CC_{50}) of the encapsulated drug was greater than 200 µg/mL, corresponding to more than 400-fold its MIC against the reference strains. Blank MPP nanoparticles were essentially non-toxic, maintaining cell viability above 95%. In contrast, free PQD-L exhibited greater cytotoxicity, with a CC_{50} of approximately 142 µg/mL. This difference suggests that nanoencapsulation may reduce non-specific cellular exposure to the drug and thereby improve its cytocompatibility. Furthermore, haemolysis remained below 5% at a concentration of 100 µg/mL, indicating good haemocompatibility. Together with the approximately 370-fold selectivity of PQD-L for bacterial DHFR over human DHFR, these findings support a favourable therapeutic window for the

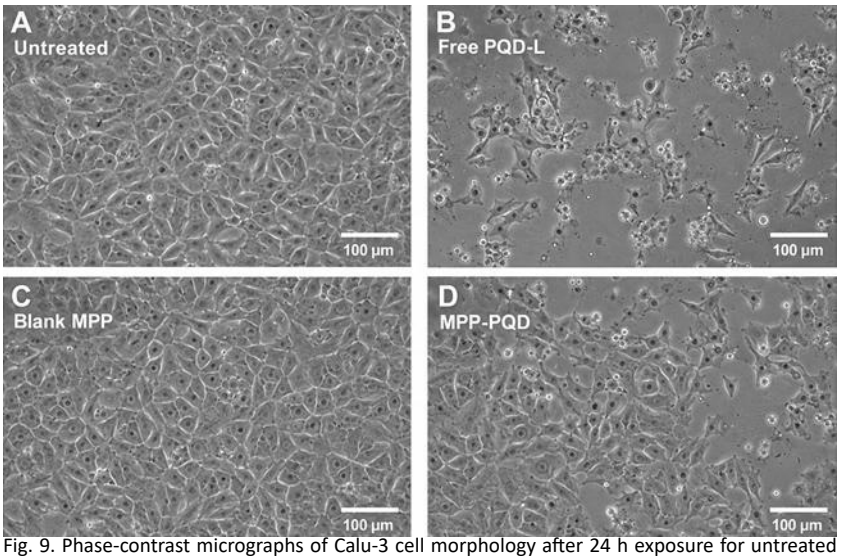


Fig. 9. Phase-contrast micrographs of Calu-3 cell morphology after 24 h exposure for untreated control, free PQD-L, blank MPP, and MPP-PQD.

Table 8. Cytocompatibility (Calu-3) and DHFR enzyme selectivity.

Agent	Viability @50 µg mL^{-1} (%)	CC_{50} (µg mL^{-1})	DHFR IC_{50} (Pa / human)	Selectivity index
MPP-PQD	88.3 ± 3.1	>200	9.2 nM / 3.4 µM	~370
Free PQD-L	71.6 ± 4.2	142 ± 9	9.2 nM / 3.4 µM	~370
Blank MPP	96.4 ± 2.0	>400		
Trimethoprim			4.6 µM / 8.1 µM	~1.8

CC BY

nanoparticle-delivered antifolate.

The central finding of this study is that a potent antibacterial compound with limited activity against MDR *P. aeruginosa* and poor delivery characteristics can be transformed into a respirable therapeutic formulation through the development of mucus-penetrating lipid–polymer hybrid nanoparticles. Each formulation component was designed to overcome a specific delivery barrier, and their combined effects account for the overall therapeutic performance observed in this study.

The selection of the antibacterial chemotype was a fundamental aspect of the formulation strategy. The resistance of all MDR isolates to trimethoprim (MIC >128 μg/mL) is consistent with the widespread occurrence of trimethoprim resistance in *P. aeruginosa* [14, 15]. The potent nanomolar inhibition of bacterial DHFR by PQD-L, together with its approximately 370-fold selectivity over the human enzyme and its retained antibacterial activity against resistant isolates, is consistent with previous reports, indicating that the 1,3-diamino-7H-pyrrolo[3,2-f]quinazoline scaffold exhibits a distinct binding mode compared with classical diaminopyrimidines, as well as membrane-perturbing and antibiofilm properties [16, 26].

Although nanoparticle-based delivery can improve drug distribution and bioavailability, it cannot compensate for the intrinsic lack of antibacterial activity. Therefore, selecting an inherently potent chemotype capable of targeting resistant bacterial strains represents an essential prerequisite for successful formulation development. The lipid–polymer hybrid architecture was designed to reconcile formulation requirements that are difficult to achieve using a single-component carrier system. The PLGA core enabled high drug encapsulation efficiency and provided a diffusion-controlled release matrix, resulting in a biphasic release profile characterized by Fickian diffusion ($n \approx 0.43$), as described by the Korsmeyer–Peppas model [20, 29]. The sustained release of PQD-L over approximately 72 h may be particularly advantageous for maintaining prolonged drug exposure at the infection site, potentially limiting the survival of slow-growing bacterial populations within biofilms. This is especially relevant because free small-molecule drugs may be rapidly cleared from the pulmonary environment. Meanwhile, the lipid interface contributed to particle stabilization by reducing aggregation and providing an anchoring platform for the PEGylated phospholipid. This enabled the incorporation of a mucus-penetrating surface during the same self-assembly process [18, 19]. These complementary properties highlight the potential advantages of hybrid nanoparticle systems over conventional liposomes or uncoated polymeric nanoparticles.

One of the most important and distinctive findings of this study was the successful development of a PEG corona capable of facilitating nanoparticle transport through mucus, a feature that has been challenging to achieve with previously investigated inhaled antibiotic nanoparticle systems. The effect of PEGylation was clearly reflected in the surface characteristics and transport behaviour of the nanoparticles. Specifically, PEGylation shifted the zeta potential from approximately −28 mV for conventional particles to nearly −8 mV for MPP-PQD, indicating effective shielding of the negatively charged PLGA surface by the PEG corona. This modification resulted in an approximately 12-fold enhancement in particle diffusivity through the reconstituted CF mucus model. Furthermore, the majority of MPP-PQD particles penetrated beyond a depth of 10 μm, whereas non-PEGylated particles remained largely immobilized within the mucus network [8-10].

This enhanced transport provides a plausible physical explanation for the improved antibiofilm performance of MPP-PQD. Effective penetration through the mucus and biofilm matrices is essential for delivering the encapsulated antibacterial agent to bacteria residing within deeper biofilm layers. Accordingly, the 4–8-fold reduction in minimum biofilm eradication concentration (MBEC) and the reduction in viable bacterial counts of up to 3.8 $\log_{10}$ observed with MPP-PQD, compared with the substantially lower activity of conventional formulations, can be partly attributed to improved nanoparticle transport. These effects may be further enhanced by the intrinsic antibiofilm properties of the PQD scaffold [26]. Notably, the mucus-penetrating formulation also demonstrated a modest improvement in planktonic antibacterial activity and aerosol performance, suggesting that reduced non-specific adhesion may provide additional benefits throughout the pulmonary drug delivery process.

The aerodynamic characteristics of MPP-PQD are also promising from a translational

CC BY

perspective. An MMAD of 3.9 µm and a fine-particle fraction exceeding 60% indicate that a substantial proportion of the nebulized dose falls within the aerodynamic size range suitable for deposition in the conducting and small airways, which are important sites of *P. aeruginosa* infection [23, 24]. Furthermore, the preservation of aerosol characteristics following nebulization suggests that PEGylation does not compromise the respirability of the formulation [35]. The favourable enzyme selectivity profile, together with the reduced cytotoxicity of encapsulated PQD-L compared with the free drug, further supports the potential for an improved therapeutic window. Direct pulmonary administration may also facilitate high local drug concentrations while limiting systemic exposure [21, 22, 25]. The lower cytotoxicity observed with MPP-PQD is consistent with the controlled-release behaviour of the formulation, which may reduce transient exposure of airway epithelial cells to high concentrations of free drug.

Despite these promising findings, several limitations should be acknowledged. First, the mucus penetration and antibiofilm experiments were performed using reconstituted mucus models and in vitro biofilms. Although these experimental systems reproduce certain aspects of the complexity of infected CF airways, they cannot fully reflect the heterogeneity, variable thickness, and immune microenvironment of patient-derived airway mucus. Therefore, further investigations using ex vivo patient sputum and in vivo infection models are necessary to confirm nanoparticle penetration and therapeutic efficacy under physiologically relevant conditions. Second, the present findings are based on a single lead compound and a defined panel of bacterial strains. The physicochemical stability of the formulation, its behaviour during dry-powder processing, and its pharmacokinetic profile and safety following repeated administration have not yet been established. In addition, potential interactions with pulmonary surfactant and alveolar macrophages require further investigation. The possibility of resistance development following prolonged exposure to subinhibitory drug concentrations should also be carefully evaluated. Finally, the results reported in this study were obtained using laboratory-scale formulations. Successful translation into clinical applications will depend on the feasibility of large-scale manufacturing, batch-to-batch reproducibility, and the development of suitable sterilization procedures. Despite these limitations, the findings demonstrate that combining an antibacterial chemotype with activity against resistant strains, a sustained-release hybrid nanoparticle core, a mucus-penetrating surface, and suitable aerosol characteristics can provide complementary and potentially synergistic therapeutic benefits. Importantly, this formulation strategy is not restricted to PQD-L and may be applicable to other poorly soluble antibacterial agents whose pulmonary delivery is limited by the combined barriers of mucus and biofilm. Thus, the proposed approach offers a potentially valuable platform for the development of inhaled antimicrobial therapies against persistent pulmonary infections, particularly those associated with multidrug-resistant *P. aeruginosa*.

CONCLUSION

In this study, we designed, synthesized, and evaluated inhalable LPHNPs for the pulmonary delivery of a lead pyrroloquinazolinediamine DHFR inhibitor against MDR *P. aeruginosa* infections. The lead compound demonstrated potent nanomolar inhibitory activity against bacterial DHFR, together with high selectivity over the human enzyme. It was successfully encapsulated within a near-neutral, respirable PEGylated hybrid nanoparticle formulation, optimized using a Box–Behnken experimental design, which exhibited high encapsulation efficiency and sustained, Fickian diffusion-controlled drug release. The dense PEG corona significantly enhanced nanoparticle diffusion through cystic fibrosis-like mucus, resulting in an approximately 10-fold improvement in antibiofilm activity and a two-fold reduction in planktonic MIC compared with the free drug, without causing appreciable cytotoxicity in human airway epithelial cells. Collectively, these findings demonstrate the potential of mucus-penetrating LPHNPs as a rational platform for pulmonary delivery of next-generation antifolate agents to infected lungs. Further investigations, including ex vivo studies using patient-derived sputum, in vivo efficacy and safety evaluations, and dry-powder formulation development, are warranted to establish the translational potential of this delivery strategy.

CONFLICT OF INTEREST

The authors declare that there is no conflict

CC BY

of interests regarding the publication of this manuscript.

REFERENCES

1. MacVicar S. World Health Organization fungal priority pathogens list. Journal of Prescribing Practice. 2024;6(7):280-281.
2. Pang Z, Raudonis R, Glick BR, Lin T-J, Cheng Z. Antibiotic resistance in Pseudomonas aeruginosa: mechanisms and alternative therapeutic strategies. Biotechnol Adv. 2019;37(1):177-192.
3. C Reygaert W. An overview of the antimicrobial resistance mechanisms of bacteria. AIMS Microbiology. 2018;4(3):482-501.
4. Moradali MF, Ghods S, Rehm BHA. Pseudomonas aeruginosa Lifestyle: A Paradigm for Adaptation, Survival, and Persistence. Frontiers in Cellular and Infection Microbiology. 2017;7.
5. Malhotra S, Hayes D, Wozniak DJ. Cystic Fibrosis and Pseudomonas aeruginosa: the Host-Microbe Interface. Clin Microbiol Rev. 2019;32(3).
6. H⍉iby N, Ciofu O, Bjarnsholt T. Pseudomonas Aeruginosa Biofilms in Cystic fibrosis. Future Microbiol. 2010;5(11):1663-1674.
7. Bjarnsholt T. The role of bacterial biofilms in chronic infections. APMIS. 2013;121(s136):1-58.
8. Suk JS, Lai SK, Wang Y-Y, Ensign LM, Zeitlin PL, Boyle MP, et al. The penetration of fresh undiluted sputum expectorated by cystic fibrosis patients by non-adhesive polymer nanoparticles. Biomaterials. 2009;30(13):2591-2597.
9. Lai SK, Wang Y-Y, Hanes J. Mucus-penetrating nanoparticles for drug and gene delivery to mucosal tissues. Adv Drug Del Rev. 2009;61(2):158-171.
10. Wang YY, Lai SK, Suk JS, Pace A, Cone R, Hanes J. Addressing the PEG Mucoadhesivity Paradox to Engineer Nanoparticles that "Slip" through the Human Mucus Barrier. Angew Chem Int Ed. 2008;47(50):9726-9729.
11. Huckaby JT, Lai SK. PEGylation for enhancing nanoparticle diffusion in mucus. Adv Drug Del Rev. 2018;124:125-139.
12. Suk JS, Xu Q, Kim N, Hanes J, Ensign LM. PEGylation as a strategy for improving nanoparticle-based drug and gene delivery. Adv Drug Del Rev. 2016;99:28-51.
13. Witten J, Samad T, Ribbeck K. Selective permeability of mucus barriers. Curr Opin Biotechnol. 2018;52:124-133.
14. Alshahrani SH, Alameri AA, Kahar F, Alexis Ramírez-Coronel A, Fadhel Obaid R, Alsaikhan F, et al. Overview of the role and action mechanism of microRNA-128 in viral infections. Microb Pathog. 2023;176:106020.
15. Wróbel A, Arciszewska K, Maliszewski D, Drozdowska D. Trimethoprim and other nonclassical antifolates an excellent template for searching modifications of dihydrofolate reductase enzyme inhibitors. The Journal of Antibiotics. 2019;73(1):5-27.
16. Li Y, Ouyang Y, Wu H, Wang P, Huang Y, Li X, et al. The discovery of 1, 3-diamino-7H-pyrrol[3, 2-f]quinazoline compounds as potent antimicrobial antifolates. Eur J Med Chem. 2022;228:113979.
17. Guan J, Zhang Q, O'Neil M, Obaldia N, Ager A, Gerena L, et al. Antimalarial Activities of New Pyrrolo[3,2-f]Quinazoline-1,3-Diamine Derivatives. Antimicrobial Agents and Chemotherapy. 2005;49(12):4928-4933.
18. Zhang L, Chan JM, Gu FX, Rhee J-W, Wang AZ, Radovic-Moreno AF, et al. Self-Assembled Lipid−Polymer Hybrid Nanoparticles: A Robust Drug Delivery Platform. ACS Nano. 2008;2(8):1696-1702.
19. Jasim SA, Ramírez-Coronel AA, Alameri AA, Sapaev IB, Mustafa YF, Turki Jalil A, et al. Phenytoin drug detection study through the B24N24 and Al24N24 nano-clusters in gas and solvent phase: DFT, TD-DFT, and thermodynamic study. Inorg Chem Commun. 2023;153:110887.
20. Danhier F, Ansorena E, Silva JM, Coco R, Le Breton A, Préat V. PLGA-based nanoparticles: An overview of biomedical applications. Journal of Controlled Release. 2012;161(2):505-522.
21. Patton JS, Byron PR. Inhaling medicines: delivering drugs to the body through the lungs. Nature Reviews Drug Discovery. 2007;6(1):67-74.
22. Sung JC, Pulliam BL, Edwards DA. Nanoparticles for drug delivery to the lungs. Trends Biotechnol. 2007;25(12):563-570.
23. Edwards DA, Hanes J, Caponetti G, Hrkach J, Ben-Jebria A, Eskew ML, et al. Large Porous Particles for Pulmonary Drug Delivery. Science. 1997;276(5320):1868-1872.
24. Ruge CA, Kirch J, Lehr C-M. Pulmonary drug delivery: from generating aerosols to overcoming biological barriers—therapeutic possibilities and technological challenges. The Lancet Respiratory Medicine. 2013;1(5):402-413.
25. Mansour H, Haemosu, Wu X. Nanomedicine in pulmonary delivery. International Journal of Nanomedicine. 2009:299.
26. Zhang Q-J, Li Y-X, Yan Y-X, Gu R-F, Zhang H-C, Zhu A-J, et al. Design, synthesis, anti-MRSA activity evaluation, and mechanism of action study of 1,3-diamino-7H-pyrrolo[3,2-f] quinazoline derivatives. Eur J Med Chem. 2026;317:119127.
27. Günday Türeli N, Türeli AE, Schneider M. Optimization of ciprofloxacin complex loaded PLGA nanoparticles for pulmonary treatment of cystic fibrosis infections: Design of experiments approach. Int J Pharm. 2016;515(1-2):343-351.
28. Ferreira SLC, Bruns RE, Ferreira HS, Matos GD, David JM, Brandão GC, et al. Box-Behnken design: An alternative for the optimization of analytical methods. Anal Chim Acta. 2007;597(2):179-186.
29. Korsmeyer RW, Gurny R, Doelker E, Buri P, Peppas NA. Mechanisms of solute release from porous hydrophilic polymers. Int J Pharm. 1983;15(1):25-35.
30. Schuster BS, Suk JS, Woodworth GF, Hanes J. Nanoparticle diffusion in respiratory mucus from humans without lung disease. Biomaterials. 2013;34(13):3439-3446.
31. Marple VA, Roberts DL, Romay FJ, Miller NC, Truman KG, Van Oort M, et al. Next Generation Pharmaceutical Impactor (A New Impactor for Pharmaceutical Inhaler Testing). Part I: Design. J Aerosol Med. 2003;16(3):283-299.
32. Al Alwan B, Alameri AA, Qasim QA, Vaqqosov S, Jawad Kadhim Z, Sivaraman R, et al. Evaluation of Structural and Thermodynamic Parameters of Dibenzothiophene Desulfurization by Carbon Nano-Filter. Polycyclic Aromatic Compounds. 2022;43(9):8252-8264.
33. Ceri H, Olson ME, Stremick C, Read RR, Morck D, Buret A. The Calgary Biofilm Device: New Technology for Rapid Determination of Antibiotic Susceptibilities of Bacterial Biofilms. J Clin Microbiol. 1999;37(6):1771-1776.
34. Al Knani ZMI, Al Ashoor AS, Hussein AN. Assessment of antioxidant activity in Vaucheria sessilis extracts and their efficacy against isolated Candida spp. from diabetic foot ulcers. Microbial Science Archives. 2023;03(03):112-119.
35. Najm MAA, Salman Abd-Alrassol K, Qasim QA, Hussein HH, Al-Salman HNK. Spectrophotometric determination of folic acid using 1,10- phenanthroline materials with ninhydrin reagent. Materials Today: Proceedings. 2022;61:865-872.

CC BY